A first-principles study of the structural and elastic properties of orthorhombic and tetragonal $Ca_3Mn_2O_7$*

Zhang Wei(张 玮)[a], and Tong Pei-Qing(童培庆)[a)b)†]

[a] Department of Physics, Institute of Theoretical Physics, Nanjing Normal University, Nanjing 210023, China
[b] Jiangsu Key Laboratory for Numerical Simulation of Large Scale Complex Systems, Nanjing Normal University, Nanjing 210023, China

(Received 4 December 2012; revised manuscript received 5 March 2013)

The structural and elastic properties of multiferroic $Ca_3Mn_2O_7$ with ferroelectric orthorhombic (O-phase) and paraelectric tetragonal structures (T-phase) have been studied by first-principles calculations within the generalized gradient approximation (GGA) and the GGA plus Hubbard U approaches (GGA + U). The calculated theoretical structures are in good agreement with the experimental values. The T-phase is found to be antiferromagnetic (AFM) and the AFM O-phase is more stable than the T-phase, which also agree with the experiments. On these bases, the single-crystal elastic constants (C_{ij}s) and elastic properties of polycrystalline aggregates are investigated for the two phases. Our elasticity calculations indicate $Ca_3Mn_2O_7$ is mechanically stable against volume expansions. The AFM O-phase is found to be a ductile material, while the AFM T-phase shows brittle nature and tends to be elastically isotropic. We also investigate the influence of strong correlation effects on the elastic properties, qualitatively consistent results are obtained in a reasonable range of values of U. Finally, the ionicity is discussed by Bader analysis. Our work provides useful guidance for the experimental elasticity measurements of $Ca_3Mn_2O_7$, and makes the strain energy calculation in multiferroic $Ca_3Mn_2O_7$ thin films possible.

Keywords: elastic constant, elastic anisotropy, strong correlation effect, multiferroic

PACS: 62.20.de, 64.30.Jk, 71.15.Mb, 71.27.+a **DOI:** 10.1088/1674-1056/22/6/066201

1. Introduction

The multiferroic materials have attracted great interest for researchers because of the peculiar physics found in these materials and the potential applications in magnetoelectronic devices. Among these materials, those with a perovskite (Pv) structure are some of the most widely studied systems such as the $BiFeO_3$[1–4] and the $TbMnO_3$.[5–8] Here we focus on the layered Pv $Ca_3Mn_2O_7$ (Fig. 1). The original interest of studying this layered Pv is mainly related to the colossal magnetoresistance (CMR) effect.[9] Recently the ferroelectricity of $Ca_3Mn_2O_7$ is studied by Benedek and Fennie.[10] It is found that the polarization of this Pv can be induced by a combination of more than one octahedron rotation mode. A new mechanism called "hybrid" improper ferroelectricity[10] is established, which opens up new ways to search for strong polarization–magnetization coupling materials. $Ca_3Mn_2O_7$ is thus considered as a promising multiferroics for practical applications.

$Ca_3Mn_2O_7$ belongs to the Ruddlesden–Popper (RP)[11] compounds $(CaO)(CaMnO_3)_n$ with $n = 2$. The n denotes the number of MnO_6 octahedron layers within a Pv block. Along the a (Fig. 1(a)) or c (Fig. 1(b)) direction, the CaO layers alternate with the Pv $(CaMnO_3)_n$ layers. The case of $n = \infty$ is exactly the Pv $CaMnO_3$. Below the Neél temperature $T_N \approx 110$ K–115 K, the crystal structure of $Ca_3Mn_2O_7$ is ferroelectric orthorhombic (Fig. 1(a), space group $Cmc2_1$, marked as O-phase) with a dominant G-type antiferromagnetic ordering (G-AFM).[13–15] At room temperature (RT), a small amount of the paraelectric tetragonal phase appears (Fig. 1(b), space group $I4/mmm$, marked as T-phase), coexisting with the majority O-phase.[15] When the temperature increases well above the RT, the crystal structure becomes a pure T-phase.[14,16] Electronic density of states (DOS) calculations show that $Ca_3Mn_2O_7$ is a direct band gap insulator, and the occupied states near the Fermi level arise mainly from the t_{2g} states of Mn.[17] The role of the two-dimensional magnetic fluctuations in $(CaO)(CaMnO_3)_n$ ($n = 1$, 2, and ∞) has also been discussed by Cardoso *et al.*[18] Despite extensive research on the magnetic and electronic properties of $Ca_3Mn_2O_7$, little is known regarding its elastic properties. Until now the single-crystal elastic stiffness constants (C_{ij}s) of the two phases are unknown from either experiments or theoretical predictions, which restricts the fabrication and fundamental understanding of $Ca_3Mn_2O_7$, such as the strain energy estimation in epitaxial thin films,[19] the stress analysis,[20] and the phase-field simulation including the elastic energy.[21–23] In addition, the elasticity of material is closely associated with various fundamental solid state properties such as the specific

*Project supported by the National Natural Science Foundation of China (Grant No. 11175087) and the Project of Graduate Students' Education and Innovation Foundation of Jiangsu Province, China (Grant No. CXZZ12_0388).

†Corresponding author. E-mail: pqtong@njnu.edu.cn

© 2013 Chinese Physical Society and IOP Publishing Ltd

heat, the phonon spectra, and the Debye temperature. Thus it is important to study the elasticity both experimentally and theoretically. In this paper, based on the density functional theory, we systematically study the structural and elastic properties of the O-phase and T-phase of $Ca_3Mn_2O_7$. In consideration of the strongly correlated nature presented in the localized 3d electrons of Mn, the influences of correlation effects on the elastic properties are studied. Through Bader analysis, we also discuss the ionicity of the two phases.

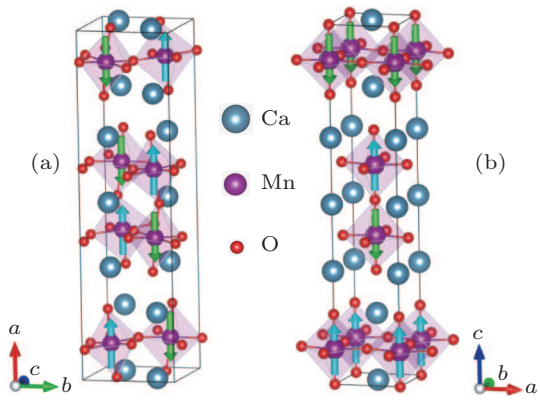


Fig. 1. (color online) Crystal structure of $Ca_3Mn_2O_7$: (a) orthorhombic phase (space group $Cmc2_1$, 48 atoms/unit cell), (b) tetragonal phase (space group $I4/mmm$, 24 atoms/unit cell). The arrows denote the directions of spins of Mn. The MnO_6 octahedrons are also sketched. This picture is generated using VESTA.[12]

The remainder of this paper is organized as follows: In Section 2 we describe the calculation method used throughout this work. Our main results will be reported in Section 3 according to the following sequence: phase stability, elastic constants, and their variations with respect to the volumes, polycrystalline elastic properties, and Bader analysis. Finally, the conclusion is given in Section 4.

2. Computational method

All the calculations are performed using the projector augmented wave (PAW) method,[24] as implemented in the VASP code.[25,26] The exchange–correlation functional is treated by the generalized gradient approximation (GGA).[27] The valence electrons configurations for Ca, Mn, and O are ($3s^2 3p^6 4s^2$), ($3p^6 3d^5 4s^2$), and ($2s^2 2p^4$), respectively. To study the influence of strong correlation effects on the elastic properties, the well-known GGA plus Hubbard U (GGA+U) method[28] is used. We use $U = 3.5$ eV.[10] For comparison, a larger value of $U = 5$ eV is also used. In the calculations of C_{ij}s (see below), several different plane wave cutoffs and/or k-meshes are tested first. We finally choose a 700-eV plane wave cutoff and a 2×4×4 Monkhorst–Pack[29] k-mesh for the O-phase (48 atoms/unit cell). For the T-phase (24 atoms/unit cell), a 700-eV plane wave cutoff and a 8×8×2 k-mesh are used.[1)] The influence of larger plane wave cutoff and/or k-mesh on the C_{ij}s are less than 1%. During the geometry optimization, the convergence criterium for electronic energy is 10^{-5} eV, and the lattices are relaxed until the Hellmann–Feynman forces are less than 0.01 eV/Å (1 Å = 0.1 nm).

The C_{ij}s are obtained using the strain-energy method. The strain tensor ε is defined as (Voigt's notation):

$$\varepsilon = \begin{pmatrix} e_1 & \frac{1}{2}e_6 & \frac{1}{2}e_5 \\ \frac{1}{2}e_6 & e_2 & \frac{1}{2}e_4 \\ \frac{1}{2}e_5 & \frac{1}{2}e_4 & e_3 \end{pmatrix}, \tag{1}$$

where (e_1,e_2,...,e_6) is a given set of strains. The deformed lattice vectors R' (3×3 matrix) are obtained by $R' = R(I+\varepsilon)$, where R is the unstrained lattice vectors and I is the 3×3 unit matrix. According to the basic elastic theory, in the vicinity of energy E_0 of the equilibrium state, the internal energy E under strain can be Taylor expanded as:

$$E = E_0 + V\sum_{i=1}^{6}\sigma_i e_i + \frac{1}{2}V\sum_{i,j=1}^{6}C_{ij}e_i e_j + \cdots, \tag{2}$$

where V is the unstrained volume, σ is the stress tensor which is defined by:

$$\sigma_i = \frac{1}{V}\left[\frac{\partial E(V,\varepsilon_j)}{\partial \varepsilon_i}\right]_{\varepsilon=0}, \tag{3}$$

and the second order elastic constants are given by

$$C_{ij} = \frac{1}{V}\left[\frac{\partial^2 E(V,\varepsilon_k)}{\partial \varepsilon_i \partial \varepsilon_j}\right]_{\varepsilon=0}. \tag{4}$$

By imposing a series of strain modes (e_1, e_2, ..., e_6), the C_{ij}s can be obtained by fitting Eq. (2). For example, C_{11} of the O-phase can be calculated by using the strain mode (δ, 0, 0, 0, 0, 0). Details of this distortion method can be found in Refs. [20] and [30] To guarantee the accuracy of fitting, for every strain mode, we apply eight successive values for the strain magnitude δ, namely, δ = ±0.02, ±0.015, ±0.01, and ±0.005.

3. Results and discussion

3.1. Structural properties and phase stability

We first report the fully relaxed equilibrium structural parameters of the O-phase with G-AFM (Fig. 1(a)) and the T-phase in Table 1. According to the experiments,[14–16] the T-phase is AFM and paramagnetic at room temperature and high temperature, respectively. Thus we consider two cases for the T-phase, i.e., magnetic and nonmagnetic (NM) cases. In the

[1)] We choose these parameters so that the two phases' total energies can converge to better than 1 meV/atom.

case of magnetic one, Matar *et al.*[17] assume a simple ferromagnetic ordering (FM) in the previous work, however we find the *A*-type AFM ordering (Fig. 1(b)) has lower energy than the FM by the generalized gradient approximation (GGA) and GGA + U calculations, thus we use *A*-AFM for the T-phase which is consistent with the experiments. From Table 1, we can see that the overall agreement between the experimental and theoretical structures is good. The lattice parameters predicted by GGA are in better agreement with the experimental values than that of GGA + U.

Table 1. Theoretical and experimental[15] lattice constants (Å), Wyckoff (Wyc.) positions of atoms (by GGA), bulk modulus B_0 (GPa) (by EOS fittings) and its pressure derivative B_0' for the AFM O-phase and AFM T-phase. The experimental values are shown in parentheses. For clarity we just give the experimental Wyc. positions of the T-phase that change after structural relaxations.

O-phase					T-phase				
	a	b	c	B_0/B_0'		a	b	c	B_0/B_0'
Expt.	(19.446)	(5.245)	(5.240)		Expt.	(3.692)	(3.692)	(19.625)	
GGA	19.466	5.292	5.302	144.15/4.98	GGA	3.772	3.772	19.257	151.27/4.85
$U = 3.5$ eV	19.473	5.325	5.349	136.84/5.08	$U = 3.5$ eV	3.788	3.788	19.334	137.55/5.42
$U = 5$ eV	19.486	5.344	5.373	129.37/5.32	$U = 5$ eV	3.808	3.808	19.344	130.14/4.45
Atom	Wyc.	x	y	z	Atom	Wyc.	x	y	z
Ca1	4*a*	0.5	0.7458	0.7149	Ca1	2*b*	0	0	0.5
		(0.5)	(0.7522)	(0.7442)					
Ca2	8*b*	0.3133	0.7427	0.7808	Ca2	4*e*	0	0	0.3163
		(0.3135)	(0.7531)	(0.7751)					(0.3145)
Mn	8*b*	0.0980	0.7489	0.7509	Mn	4*e*	0	0	0.0994
		(0.0974)	(0.7532)	(0.7500)					(0.0978)
O1	4*a*	0	0.6883	0.7602	O1	2*a*	0	0	0
		(0)	(0.7001)	(0.7562)					
O2	8*b*	0.0856	0.0396	0.9602	O2	4*e*	0	0	0.1975
		(0.0882)	(0.0392)	(0.9609)					(0.1941)
O3	8*b*	0.1092	0.5386	0.0378	O3	8*g*	0	0.5	0.0975
		(0.1044)	(0.5339)	(0.0271)					(0.1020)
O4	8*b*	0.1958	0.7958	0.7432					
		(0.1952)	(0.7808)	(0.7471)					

In order to study the phase stability, we calculate the total energies with respect to the volumes in Fig. 2. For each selected volume, after relaxation, it is found that the deviations of the stress tensors from a diagonal hydrostatic form are all less than 1 kbar (0.1 GPa, 1 bar = 100 kPa), indicating the applied external pressures are isotropic. Then the calculated total energies E and volumes V are fitted by the third-order Birch–Murnaghan[31] equation of state (EOS),

$$E(V) = -\frac{9}{16}B_0\left[(4-B_0')\frac{V_0^3}{V^2} - (14-3B_0')\frac{V_0^{7/3}}{V^{4/3}} + (16-3B_0')\frac{V_0^{5/3}}{V^{2/3}}\right] + E_0, \quad (5)$$

where V_0, E_0, B_0, B_0' are the resulted equilibrium volume, equilibrium energy, bulk modulus, and the pressure derivative of bulk modulus, respectively. The NM T-phase has larger B_0 (160.16 GPa by EOS) and smaller equilibrium volume (see Fig. 2) than the AFM O-phase and T-phase, indicating the NM T-phase is harder. Both the AFM O-phase and T-phase are very close in the B_0 especially when the strong correlation effects are included, indicating the similar ability in the resistance to isotropic compression. From Fig. 2 we can see that the local magnetic moments of Mn (M) show decreasing trends with decreasing volumes. The GGA predicted M of the AFM O-phase at the equilibrium structure is ~2.59 μ_B, which is consistent with the experimental value (2.62 μ_B~2.72 μ_B).[15] The including of strong correlation effects makes the M show increasing trend ($M = 3$ (3.21) μ_B by GGA + U with $U = 3.5$ (5) eV), and thus the M deviates from the experiment. Figure 2 also shows that the NM T-phase is not stable relative to the AFM T-phase and AFM O-phase. The total energy of the AFM O-phase is 38.93 meV/atom (39.21 (39.71) meV/atom by GGA + U with $U = 3.5$ (5) eV) lower than the AFM T-phase, indicating the AFM O-phase is more stable than the T-phase which agrees with the experiments.[13–16] The total energy contains the electronic energy and the interaction energy between ions. By carefully comparing the component of the total energies of the two phases, we find that although the AFM T-phase has lower electronic energy than the AFM O-phase, the interaction energy between ions of the AFM O-phase is much lower than that of the AFM T-phase. Therefore the AFM O-phase's lower interaction energy between ions is the dominant reason why AFM O-phase is more stable than the AFM T-phase.

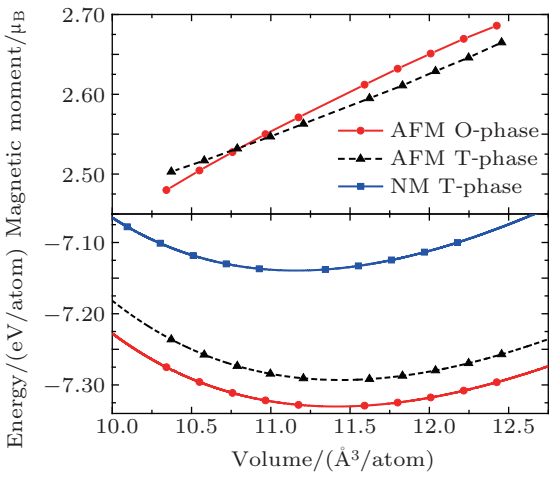


Fig. 2. (color online) GGA-calculated total energies and magnetic moments of Mn for the O-phase and T-phase of $Ca_3Mn_2O_7$ as a function of volume. The energy versus volume curves are fitted by the third-order Birch–Murnaghan equation of state (EOS).

3.2. Single-crystal C_{ij}s and polycrystalline elastic properties

Now, let us show the results of elastic calculations. The orthorhombic and tetragonal crystal systems have nine and six independent C_{ij}s, respectively. The predicted C_{ij}s for the O-phase (AFM) and T-phase (AFM/NM) by GGA and GGA + U are listed in Table 2. We can see that all the C_{ij}s of the AFM T-phase decrease with increasing U, while the C_{11}, C_{55}, and C_{66} of the O-phase increase at first, then decrease. To examine the influence of these variations of C_{ij}s on the mechanical stability, we reference the well-known Born–Huang stability criteria[32] for the O-phase:

$$\begin{aligned} &C_{11}>0,\ C_{22}>0,\ C_{33}>0,\ C_{44}>0,\\ &C_{55}>0,\ C_{66}>0,\ (C_{11}+C_{22}-2C_{12})>0,\\ &(C_{11}+C_{22}+C_{33}+2C_{12}+2C_{13}+2C_{23})>0,\\ &(C_{11}+C_{33}-2C_{13})>0,\ (C_{22}+C_{33}-2C_{23})>0, \end{aligned} \quad (6)$$

and for the T-phase:

$$\begin{aligned} &(2C_{11}+C_{33}+2C_{12}+4C_{13})>0,\\ &C_{11}>0,\ C_{33}>0,\ C_{44}>0,\ C_{66}>0,\\ &(C_{11}-C_{12})>0,\ (C_{11}+C_{33}-2C_{13})>0. \end{aligned} \quad (7)$$

Table 2. GGA and GGA + U calculated single-crystal C_{ij}s (GPa) for the O-phase (AFM) and T-phase (AFM/NM) at the equilibrium volume. The results of NM T-phase are shown in parentheses.

	O-phase				T-phase		
C_{ij}	$U=0$ eV	$U=3.5$ eV	$U=5$ eV	C_{ij}	$U=0$ eV	$U=3.5$ eV	$U=5$ eV
C_{11}	245.166	248.811	242.809	C_{11}	305.649 (280.032)	267.496	265.031
C_{12}	126.763	113.497	106.853	C_{12}	67.568 (159.259)	56.549	45.967
C_{13}	110.060	95.941	88.178	C_{13}	88.550 (94.501)	81.191	75.574
C_{22}	223.252	215.900	206.453				
C_{23}	94.734	93.122	86.885				
C_{33}	210.071	202.234	191.620	C_{33}	285.819 (245.967)	281.988	278.956
C_{44}	97.910	97.461	94.427	C_{44}	81.683 (83.927)	81.556	78.477
C_{55}	85.305	85.859	83.060				
C_{66}	84.118	84.552	82.053	C_{66}	81.814 (89.762)	78.767	78.095

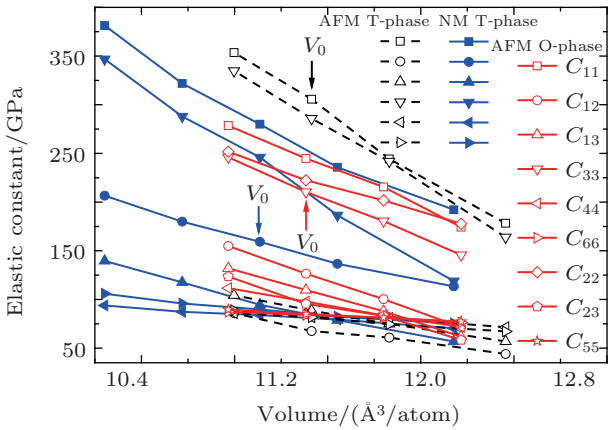


Fig. 3. (color online) GGA-calculated elastic stiffness constants for the O-phase and T-phase of $Ca_3Mn_2O_7$ as a function of volume. The arrows denote the equilibrium volume V_0. Note that we have C_{44} = C_{55} for the T-phase.

From Table 2 we can see that all the predicted C_{ij}s by GGA and GGA + U satisfy these conditions, indicating both the O-phase and T-phase are mechanically stable at zero pressure. It is known that the increasing temperature, in general, expands the volume. To see whether $Ca_3Mn_2O_7$ is mechanically stable at larger volumes, we calculate the C_{ij}s with respect to the volumes in Fig. 3. We can see that the C_{11} and C_{33} decrease sharply with increasing volumes, while the C_{55} and C_{66} decrease slightly with increasing volumes. Even so, the C_{ij}s still satisfy the above stability criteria. The same trend and stability are also predicted by GGA + U. Thus $Ca_3Mn_2O_7$ is mechanically stable against volume expansions.

3.3. Polycrystalline elastic properties

Next, with the aim to study the elastic properties of polycrystalline $Ca_3Mn_2O_7$ at larger length scales, we investigate the polycrystalline elastic properties including the shear mod-

ulus, Young's modulus, Poisson ratios, etc. according to the Voigt–Reuss–Hill[33–35] approximation. In Voigt theory, the bulk and shear modulus are calculated from singe-crystal $C_{\rm ij}$s as follows:

$$\begin{aligned} B_{\rm V} &= \frac{2}{9}(C_{12}+C_{23}+C_{13})+\frac{1}{9}(C_{11}+C_{22}+C_{33}),\\ G_{\rm V} &= \frac{1}{5}(C_{44}+C_{55}+C_{66})\\ &\quad -\frac{1}{15}(C_{12}+C_{23}+C_{13})+\frac{1}{15}(C_{11}+C_{22}+C_{33}), \quad (8) \end{aligned}$$

while in Reuss theory:

$$\begin{aligned} \frac{1}{B_{\rm R}} &= 2(S_{12}+S_{23}+S_{13})+S_{11}+S_{22}+S_{33},\\ \frac{1}{G_{\rm R}} &= \frac{1}{5}(S_{44}+S_{55}+S_{66})\\ &\quad -\frac{4}{15}(S_{12}+S_{23}+S_{13})+\frac{4}{15}(S_{11}+S_{22}+S_{33}), \quad (9) \end{aligned}$$

where S_{ij}s represent the elastic compliance constants, i.e., the inverse matrix of C_{ij}s. Then the elastic modulus of the polycrystalline aggregates can be got by Hill's average: $B_{\rm H}=\frac{1}{2}(B_{\rm V}+B_{\rm R})$, $G_{\rm H}=\frac{1}{2}(G_{\rm V}+G_{\rm R})$. The Poisson's ratio ν, Young's modulus Y are calculated by the following relations[36]

$$Y=\frac{9BG}{3B+G}, \quad \nu=\frac{3B-2G}{2(3B+G)}. \quad (10)$$

All the calculated results are summarized in Table 3. The NM T-phase shows different elastic characters from the AFM T-phase due to the influence of magnetism. Since the AFM T-phase is obviously more stable in energy than the NM one and for the study of strong correlation effects on the elastic properties, we focus our discussion on the AFM T-phase hereafter. It can be seen that the bulk modulus calculated by C_{ij}s are close to that by EOS fittings (Table 1), indicating the reliability of the calculations of C_{ij}s. The EOS fitted bulk moduli are 1.8%∼2.59% lower than that ($B_{\rm H}$) by C_{ij}s, which can be attributed to: (i) the determinations of C_{ij}s are in the fully elastic region, while the EOS fittings are not. (ii) In the calculations of C_{ij}s the cell shape is fixed and only the atomic positions are allowed to relax, while in the EOS fittings both the cell shape and atomic positions are relaxed. The AFM O-phase has lower shear modulus and Young's modulus than that of the AFM T-phase, which means the AFM T-phase has higher resistance to the deformations upon shear and uniaxial stresses. For both the O-phase and the T-phase, all the moduli decrease with increasing U except for the shear and Young's modulus of the AFM O-phase. The B/G ratio also shows a decreasing trend. According to Pugh's criteria,[37] a critical value of B/G ratio of about 1.75 can separate brittle and ductile materials. A B/G value lower than about 1.75 indicates a brittle nature of the material whereas a higher value is associated with better ductility. As shown in Table 3, the AFM T-phase is a brittle material, while the AFM O-phase shows ductile nature even when the U increases to 5 eV. The elastic anisotropy is closely associated with the possibility to induce microcracks[38] into materials, which has a significant application in engineering science. It is thus necessary to calculate the elastic anisotropy so as to understand the characteristics and to improve the durability of materials. Here two criteria are used for analysis. The first are the general definitions proposed by Chung and Buessem,[39] which is based on the differences between $B_{\rm V}$ ($B_{\rm R}$) and $G_{\rm V}$ ($G_{\rm R}$):

$$A_{\rm B}=\frac{B_{\rm V}-B_{\rm R}}{B_{\rm V}+B_{\rm R}}, \quad A_{\rm G}=\frac{G_{\rm V}-G_{\rm R}}{G_{\rm V}+G_{\rm R}}. \quad (11)$$

Table 3. GGA and GGA + U calculated polycrystal aggregate properties of bulk modulus B (GPa), shear modulus G (GPa), Young's modulus Y (GPa), B/G ratio, Poisson's ratio ν in Hill approach, the anisotropy ratio $A_{\rm B}$ and $A_{\rm G}$ (percent values) and universal anisotropy index A^U for the O-phase (AFM) and T-phase (AFM/NM) at the equilibrium volume. The right subscripts V, R, and H denote the values got by Voigt theory, Reuss theory, and Hill approximation, respectively. The results of NM T-phase are shown in parentheses.

	O-phase			T-phase		
Property	$U=0$ eV	$U=3.5$ eV	$U=5$ eV	$U=0$ eV	$U=3.5$ eV	$U=5$ eV
$B_{\rm V}$	149.067	141.341	133.857	154.050 (166.950)	139.427	133.694
$B_{\rm R}$	146.898	139.417	131.677	154.050 (163.028)	138.823	132.951
$G_{\rm V}$	76.596	77.867	75.839	92.533 (82.041)	88.245	87.803
$G_{\rm R}$	72.611	74.589	72.744	90.471 (79.825)	87.110	86.106
$Y_{\rm V}$	196.185	197.358	191.375	231.289 (211.482)	218.615	216.102
$Y_{\rm R}$	187.018	189.902	184.294	226.979 (205.873)	216.125	212.452
$B_{\rm H}$	147.982	140.379	132.767	154.050 (164.989)	139.125	133.323
$G_{\rm H}$	74.603	76.228	74.291	91.502 (80.933)	87.678	86.954
$Y_{\rm H}$	191.610	193.635	187.838	229.138 (208.678)	217.370	214.278
$B_{\rm H}/G_{\rm H}$	1.984	1.842	1.787	1.684 (2.039)	1.587	1.533
$\nu_{\rm H}$	0.284	0.270	0.264	0.252 (0.289)	0.240	0.232
$A_{\rm B}(\%)$	0.733	0.685	0.821	0 (1.189)	0.217	0.279
$A_{\rm G}(\%)$	2.671	2.150	2.083	1.127 (1.369)	0.647	0.976
A^U	0.289	0.233	0.229	0.114 (0.163)	0.070	0.104

The second is the universal elastic anisotropy index A^U,[40] which is recently proposed by Ranganathan and Ostoja–Starzewski with

$$A^U = 5\frac{G_V}{G_R} + \frac{B_V}{B_R} - 6.$$

A^U is zero for locally isotropic single crystal. The departure of A^U from zero reflects the extent of single-crystal anisotropy including both the shear and bulk contributions. As shown in Table 3, both the two criteria give qualitatively consistent results regardless of the variations of U. The AFM O-phase is obviously anisotropic with respect to the AFM T-phase, indicating the AFM O-phase is more prone to cause stress concentration and microcracks relative to the AFM T-phase. The A^U of the AFM T-phase ranges from 0.07 to 0.114, indicating the AFM T-phase tends to be elastically isotropic, while the AFM O-phase shows similar elastic anisotropy nature to hexagonal-close-packed (hcp) Hg, hcp Mg, and face-centered-cubic (fcc) Rh with $A^U \approx 0.22\sim0.28$.[41]

3.4. Bader charges analysis

Finally, to numerically estimate the amount of electrons transferred between various atoms, we carry out the Bader analysis.[42,43] In Bader analysis, each atom is divided by a zero flux surface, where the charge density reaches a minimum perpendicular to this surface. The charge (Q_B, Bader charge) integrated within this region (V_B, Bader volume) is a good approximation to estimate the total electronic charge of an atom. The advantages of this methodology are: i) it has the consistent mathematical definition of atomic volumes, and ii) it is independent of basis sets.[43] From Bader analysis, we also can get the minimum distance d_{min} from each atom to the surface. To meet the precision of charge density calculations, we use the grids which are four times finer than the default values, i.e., (672×192×192) for the O-phase and (144×144×672) for the T-phase. Since the using of GGA + U just slightly changes the value of Q_B which does not affect the qualitative explanations, we show the results calculated by GGA. As displayed in Table 4, the different values of ΔQ_B of the same kind of atoms indicate the different surroundings of the congeneric atoms, reflecting the distortions of local structures. We also can see from Table 4 that the two phases' charge distributions of atoms are quite similar, thus the distributions of valence electrons have little to do with the two phases' differences of elastic properties. Considering the numbers of valence electrons of Ca, Mn, and O atoms (10, 13, and 6 respectively), averagely about 1.57 and 1.82 electrons transfer from each of Ca and Mn atoms to O atom. Comparing with the nominal charges of Ca (+2), Mn (+4), and O (−2) according to the pure ionic model, relatively, the Ca–O bonds are quite ionic, while the Mn–O bonds are more covalent, which is consistent with the DOS calculations that the Mn 3d states hybridize with the O 2p states in the valence bands.[17] Therefore, approximately, $Ca_3Mn_2O_7$ can be expressed as $Ca^{1.57+}Mn^{1.82+}O^{1.19-}$.

Table 4. GGA calculated charge loss (ΔQ_B, –) or gain (ΔQ_B, +) of each atom, the minimum distances d_{min} to the Bader surfaces and the Bader volumes V_B for the AFM O-phase and AFM T-phase.

O-phase					T-phase				
Atom	Wyc.	$\Delta Q_B/e$	d_{min}/Å	V_B/Å^3	Atom	Wyc.	$\Delta Q_B/e$	d_{min}/Å	V_B/Å^3
Ca1	4*a*	–1.5743	1.1414	11.2590	Ca1	2*b*	–1.5960	1.2760	11.8293
Ca2	8*b*	–1.5400	1.1068	11.9010	Ca2	4*e*	–1.5516	1.1336	12.0237
Mn	8*b*	–1.8197	0.9084	6.9684	Mn	4*e*	–1.8150	0.9167	6.8048
O1	4*a*	+1.1627	0.9459	11.8253	O1	2*a*	+1.1577	0.9456	11.8004
O2	8*b*	+1.1553	0.9228	11.4130	O2	4*e*	+1.2443	0.9373	15.3042
O3	8*b*	+1.1428	0.9093	11.3618	O3	8*g*	+1.1707	0.9430	11.2681
O4	8*b*	+1.2673	0.9432	15.0819					

4. Conclusion

In summary, we have studied the structural and elastic properties of orthorhombic and tetragonal $Ca_3Mn_2O_7$ using the GGA and GGA + U approaches. Our calculations show that the T-phase is AFM and the O-phase is energetically more stable than the T-phase, which are in agreement with the experiments. The AFM O-phase shows a ductile nature and has lower shear modulus and Young's modulus than the AFM T-phase, while the AFM T-phase is a brittle material and tends to be elastically isotropic. The NM T-phase is found to be harder than the AFM T-phase and O-phase due to its smaller equilibrium volume and larger bulk modulus. All the three phases are predicted to be mechanically stable against volume expansions. Qualitatively, the elastic properties of $Ca_3Mn_2O_7$ are not affected by the strong correlation effects in a reasonable range of values of U. By Bader analysis, we conclude that the Ca–O bonds are quite ionic while the Mn–O bonds are more covalent, and $Ca_3Mn_2O_7$ can approximately be expressed as $Ca^{1.57+}Mn^{1.82+}O^{1.19-}$. Our work provides useful guidance

for the experimental elasticity measurements, and makes the strain energy calculation in multiferroic $Ca_3Mn_2O_7$ thin films possible.

References

[1] Wang J, Neaton J B, Zheng H, Nagarajan V, Ogale S B, Liu B, Viehland D, Vaithyanathan V, Schlom D G, Waghmare U V, Spaldin N A, Rabe K M, Wuttig M and Ramesh R 2003 *Science* **299** 1719

[2] Neaton J B, Ederer C, Waghmare U V, Spaldin N A and Rabe K M 2005 *Phys. Rev. B* **71** 014113

[3] Ederer C and Neaton J B 2005 *Phys. Rev. B* **71** 060401(R)

[4] Diéguez O and Íñiguez J 2011 *Phys. Rev. Lett.* **107** 057601

[5] Kimura T, Goto T, Shintani H, Ishizaka K, Arima T and Tokura Y 2003 *Nature* **426** 55

[6] Xiang H J, Wei S H, Whangbo M H and Da Silva J L F 2008 *Phys. Rev. Lett.* **101** 037209

[7] Malashevich A and Vanderbilt D 2009 *Phys. Rev. B* **80** 224407

[8] Rovillain P, Cazayous M, Gallais Y, Measson M A, Sacuto A, Sakata H and Mochizuki M 2011 *Phys. Rev. Lett.* **107** 027202

[9] Kimura T, Tomioka Y, Kuwahara H, Asamitsu A, Tamura M and Tokura Y 1996 *Science* **274** 1698

[10] Benedek N A and Fennie C J 2011 *Phys. Rev. Lett.* **106** 107204

[11] Ruddlesden S N and Popper P 1957 *Acta Crystallogr.* **10** 538

[12] Momma K and Izumi F 2008 *J. Appl. Crystallogr.* **41** 653

[13] Guiblin N, Grebille D, Leligny H and Martin C 2002 *Acta Crystallogr. Sect. C* **58** i3

[14] Bendersky L A, Greenblatt M and Chen R 2003 *J. Solid State Chem.* **174** 418

[15] Lobanov M V, Greenblatt M, Caspi E N, Jorgensen J D, Sheptyakov D V, Toby B H, Botez C E and Stephens P W 2004 *J. Phys.: Condens. Matter* **16** 5339

[16] Fawcett I D, Sunstrom IV J E, Greenblatt M, Croft M and Ramanujachary K V 1998 *Chem. Mater.* **10** 3643

[17] Matar S F, Eyert V, Villesuzanne A and Whangbo M H 2007 *Phys. Rev. B* **76** 054403

[18] Cardoso C, Borges R P, Gasche T and Godinho M 2008 *J. Phys.: Condens. Matter* **20** 035202

[19] Shen J Y, Johnston S, Shang S L and Anderson T 2002 *J. Cryst. Growth* **240** 6

[20] Gressmann T, Wohlschlögel M, Shang S L, Welzel U, Leineweber A, Mittemeijer E J and Liu Z K 2007 *Acta Mater.* **55** 5833

[21] Chen L Q 2002 *Ann. Rev. Mater. Res.* **32** 113

[22] Zhang J X, Li Y L, Wang Y, Liu Z K, Chen L Q, Chu Y H, Zavaliche F and Ramesh R 2007 *J. Appl. Phys.* **101** 114105

[23] Sheng G, Hu J M, Zhang J X, Li Y L, Liu Z K and Chen L Q 2012 *Acta Mater.* **60** 3296

[24] Blöchl P E 1994 *Phys. Rev. B* **50** 17953

[25] Kresse G and Furthmüller J 1996 *Phys. Rev. B* **54** 11169

[26] Kresse G and Joubert D 1999 *Phys. Rev. B* **59** 1758

[27] Perdew J P, Burke K and Ernzerhof M 1997 *Phys. Rev. Lett.* **78** 1396

[28] Dudarev S L, Botton G A, Savrasov S Y, Humphreys C J and Sutton A P 1998 *Phys. Rev. B* **57** 1505

[29] Monkhorst H J and Pack J D 1976 *Phys. Rev. B* **13** 5188

[30] Beckstein O, Klepeis J E, Hart G L W and Pankratov O 2001 *Phys. Rev. B* **63** 134112

[31] Birch F 1947 *Phys. Rev.* **71** 809

[32] Born M and Huang K 1988 *Dynamical Theory of Crystal Lattices* (New York: Oxford University Press)

[33] Voigt D W 1928 *Lehrbuch der Kristallphysik* (Leipzig: Teubner Press)

[34] Reuss A and Angew Z 1929 *Math. Mech.* **9** 55

[35] Hill R 1952 *Proc. Phys. Soc. Sect. A* **65** 349

[36] Schneider E, Anderson O L and Soga N 1974 *Elastic Constants and Their Measurement* (New York: McGraw-Hill Press)

[37] Pugh S F 1954 *Phil. Mag.* **45** 823

[38] Tvergaard V and Hutchinson J W 1988 *J. Am. Ceram. Soc.* **71** 157

[39] Chung D H and Buessem W R 1968 *Anisotropy in Single Crystal Refractory Compounds* (New York: Plenum)

[40] Ranganathan S I and Ostoja-Starzewski M 2008 *Phys. Rev. Lett.* **101** 055504

[41] Shang S L, Saengdeejing A, Mei Z G, Kim D E, Zhang H, Ganeshan S, Wang Y and Liu Z K 2010 *Comput. Mater. Sci.* **48** 813

[42] Bader R F W 1990 *Atoms in Molecules: A Quantum Theory* (Oxford: Oxford University Press)

[43] Tang W, Sanville E and Henkelman G 2009 *J. Phys.: Condens. Matter* **21** 084204